RSC Advances

ROYAL SOCIETY OF CHEMISTRY

www.rsc.org/advances

Porous aerogel nanocomposite of silver nanoparticles-functionalized cellulose nanofibrils for SERS detection and catalytic degradation of Rhodamine B

Soon Wei Chook[a,*], Chin Hua Chia[a,*] Chi Hoong Chan[a], Siew Xian Chin[a], Sarani Zakaria[a], Mohd Shaiful Sajab[a,b], Nay Ming Huang[c].

[a] *Bioresources and Biorefinery Laboratory, School of Applied Physics, Faculty of Science and Technology, Universiti Kebangsaan Malaysia, 43600 Bangi, Selangor, Malaysia*
[b] *Research Center for Sustainable Process Technology (CESPRO), Faculty of Engineering and Built Environment, Universiti Kebangsaan Malaysia, 43600 Bangi, Selangor, Malaysia*
[c] *Low Dimensional Materials Research Centre, Department of Physics, Faculty of Science, University Malaya, 50603 Lembah Pantai, Kuala Lumpur, Malaysia*

* Corresponding authors: S.W. Chook (chooksoonwei@gmail.com) and C.H. Chia (chia@ukm.edu.my)

Abstract
Herein, cellulose nanofibril (CNF) was functionalised with silver nanoparticles (AgNPs) via a green *in situ* hydrothermal synthesis approach. The presence of active functional groups on the CNF favours the direct synthesis and growth of AgNPs on the nanofibrils without the use of external reducing agent. The freeze-dried CNF-AgNPs aerogel nanocomposite exhibited a highly porous structure, as revealed by FESEM. An organic dye, Rhodamine B (RhB), was chosen to investigate the characteristics of the produced nanocomposite. Detection of the dye via Raman spectroscopy and analysis of catalysis capabilities by degradation of the dye were used to define nanocomposite properties. The nanocomposite showed significant enhancement in detection of signal for RhB in aqueous solution, as compared to the neat CNF, which is attributed to the surface-enhanced Raman scattering effect (SERS) of the immobilized AgNPs. Moreover, the CNF-AgNPs nanocomposite also showed sensitivity for detecting RhB at different concentrations, ranging from 5×10^{-3} M to 5×10^{-7} M. In addition, the nanocomposite exhibited a notable catalytic effect on the degradation of RhB in the presence of sodium borohydride.

Keywords: Aerogel, catalyst, nanocomposite, SERS

Introduction
To date, water pollutions remain one of the major environmental disasters as a consequence of continued and reckless human activities. Untreated wastewater discharged from textile, packaging, and printing industries containing dye compounds has drawn public concern, as some of the dye compounds have been proven to be harmful not only towards aquatic ecosystem, but also to human health as well[1, 2]. Therefore, it is essential to develop a multifunctional material that could

effectively monitor, detect, and remove these hazardous pollutants from the environment. In light of the rapid development of nanotechnology, nanomaterials have emerged as a promising class of material for efficient wastewater remediation due to their high specific surface area that allows for more effective interactions with pollutants[3-5].

Silver nanoparticles (AgNPs) have been of great interest to researchers due to their combination of unique and intriguing physicochemical characteristics with exceptional antimicrobial abilities, which have been widely explored for vast array of applications. For instance, AgNPs have been incorporated into different polymeric matrices for effective water disinfection[6, 7]. In addition, large amounts of research have focused on surface-enhanced Raman scattering (SERS), a technique used in Raman spectroscopy by utilizing AgNPs to enhance the weak scattered Raman signal for analysis and detection of environmental pollutants, biological and chemical compounds[8, 9]. AgNPs have also been widely used as heterogeneous catalysts for reduction of chemical compounds, including organic dyes and nitroaromatic compounds in the presence of sodium borohydride[10-13].

A general and popular strategy to expand the practical applicability of AgNPs is through immobilization or incorporation of AgNPs onto a substrate or matrix, which can facilitate the recovery of AgNPs, while preventing leaching of nanoparticles into the environment. Owing to its abundance and biocompatibility, a large number of reported studies have utilized cellulosic materials for the immobilizations of AgNPs[14-16]. *In situ* immobilization is a facile and extensively adopted method for fabrication of cellulose-AgNPs composites, which involve interactions between Ag precursors and cellulose, followed by introduction of a reducing agent to facilitate the formation of AgNPs on the cellulose[16, 17]. Alternatively, a greener approach has also been developed by using cellulose as the reducing and stabilizing agent[18, 19], without involving the use of conventional and hazardous reducing agents, such as formaldehyde and hydrazine hydrates[20, 21]. This activity can be accounted for by the large number of repeating units of reducing sugars within the macromolecular structure of cellulose.

Nanocelluloses, including bacterial cellulose[18], cellulose nanocrystal[22, 23], and cellulose nanofibril (CNF)[24, 25], have emerged as attractive candidates that possesses many advantages for immobilization of AgNPs, including high surface area and abundant reactive functional groups. CNF is a nanocellulose with a high aspect ratio, which can be obtained from defibrillation of cellulose to elementary fibrils. Various chemical pre-treatment methods have been developed to produce CNF, namely 2,2,6,6-tetramethylpiperidine-1-oxyl radical (TEMPO) mediated oxidation [26], periodate-chlorite oxidation [27], enzymatic reactions [28], and acidified chlorite [29]. In a recent study, acidified chlorite bleaching combined with a disintegration method was employed to produce kenaf CNF with excellent capabilities for rapid removal of methylene blue from aqueous solution via adsorption,

due to its high hemicelluose content[30]. In particular, the main component of the produced CNF consists of repeating units of β(1→4)-D-glucopyranose from cellulose alongside β(1→4)-D-xylopyranose and 4-O-methylglucuronic acid from hemicellulose[30].

Herein, we describe a facile and green *in situ* synthesis approach to functionalize CNF with AgNPs and produce a porous sponge-like aerogel nanocomposite for environmental remediation applications. Rhodamine B (RhB), a hazardous fluorescence organic dye used in textile and biomedical industries[31, 32], was selected as the model analyte for SERS detection and catalytic degradation.

Experimental

Materials

Kenaf core (KC) powder (60–80 mesh) was obtained from Malaysian Agricultural Research and Development Institute (MARDI). Sulphuric acid (H_2SO_4, 98%, HmbG Chemicals), sodium chlorite ($NaClO_2$, 80%, Acros Organics), glacial acetic acid ($C_2H_4O_2$, 95%, R&M Chemicals), hydrochloric acid (HCl, 32%, JT Baker), Rhodamine B ($C_{28}H_{31}ClN_2O_3$, Sigma-Aldrich), sodium borohydride ($NaBH_4$, 99%), and silver nitrate ($AgNO_3$, 99%) were purchased from Merck. All the chemicals were analytical grade and used as received without further purification.

Fabrication of CNF-AgNPs nanocomposite

Kenaf CNF was prepared via an acidified chlorite bleaching method followed with high-speed agitation, according to a previous described procedure[30]. Then, 0.2 M of $AgNO_3$ solution was prepared and added to 30 g of CNF suspension (0.7 wt.%). The mixture of CNF and $AgNO_3$ was stirred in the dark for 30 min and subsequently centrifuged to separate the supernatant containing unattached and excessive $AgNO_3$ on the fibres. After this step, 20 mL of deionized water was added to the precipitated CNF and stirred for 10 min to disperse the precipitated CNF. The CNF suspension was then poured into a 50 mL Teflon lined autoclave, which was sealed and placed into a conventional oven, and heated at 130˚C for 2.5 h. The autoclave was removed from the oven after the reaction and cooled with flowing water. The resulting yellowish material was collected and washed using deionized water by centrifugation at 8000 rpm for 10 min to remove excessive and unreacted Ag ions. The samples was rapidly frozen in a cooling chamber at −105˚C and subjected to freeze drying for two days. The dried samples were stored in dry and dark conditions prior to the characterization and testing procedures.

Characterizations

The ultraviolet-visible spectra of the CNF and CNF-AgNPs suspensions were recorded using an Ultraviolet-visible spectrophotometer (UV–vis, Jenway 7315). The formation of AgNPs on CNF was further verified using a Transmission electron microscope (TEM, Philips CM-12). The nanocomposite was characterized using a X-ray diffractometer (XRD, Bruker Advance). The structure and morphology of the

nanocomposite was observed under a Field emission scanning electron microscope (FESEM, Zeiss Merlin Compact). For the SERS tests, 10 mg of CNF-AgNPs was immersed in different concentrations of RhB solution for 30 min. The nanocomposites were removed and dried at 60 ˚C. The Raman spectra of nanocomposites with RhB were acquired using a Raman spectroscopy (Renishaw inVia Raman microscope) from 400 to 1800 cm^{-1}. For the catalytic degradation experiments, different amounts of CNF-AgNPs aerogel (10, 30, and 60 mg) were added in a 50 mL of 1.0×10^{-4} M RhB. The mixtures were left for 5 min before the addition of 1.0 mL $NaBH_4$ (0.1 M) under atmospheric conditions. The absorbance value at wavelength 554 nm at different time intervals was recorded using the UV-vis spectrophotometer. The concentrations of the RhB were calculated based on a calibration curve of absorbance values versus dye concentrations. Additionally, different concentrations of RhB (2.0×10^{-4}, 1.0×10^{-4} and 4.0×10^{-5} M) were prepared and 10 mg CNF-AgNPs was added, followed by the addition of 1.0 mL of 0.1 M $NaBH_4$ to study the efficiency of RhB dye degradation.

Results and discussion

Preparation and characterizations of CNF-AgNPs

The successful preparation of CNF-AgNPs nanocomposite using the *in situ* hydrothermal method was examined via UV-vis spectrophotometry, XRD, and TEM. Fig. 1 shows the UV-vis spectra of the neat CNF and the CNF-AgNPs suspensions. The CNF suspension was transformed from colourless to yellowish (inset of Fig. 1a) by the hydrothermal process, indicating the successful formation of AgNPs. In this case, CNF acted as a reducing agent for the formation of AgNPs. The absorption peak recorded at 420 nm corroborates the formation of AgNPs due to the localized surface plasmon resonance (LSPR) effect of AgNPs as a result of the collective oscillation of conduction electrons that occurred when AgNPs interacting with light[33]. The XRD diagrams of both CNF and CNF-AgNPs, shown in Fig. 1b, exhibit a typical diffraction pattern of cellulose I. Additionally, the peaks indicated by the arrows corresponded to the (111), (200), (220), and (311) forms of face-centered-cubic of Ag crystal (JCPDS file no. 04-0783). That these were found in the CNF-AgNPs sample, which further demonstrates the formation of crystallite AgNPs via the *in situ* hydrothermal method.

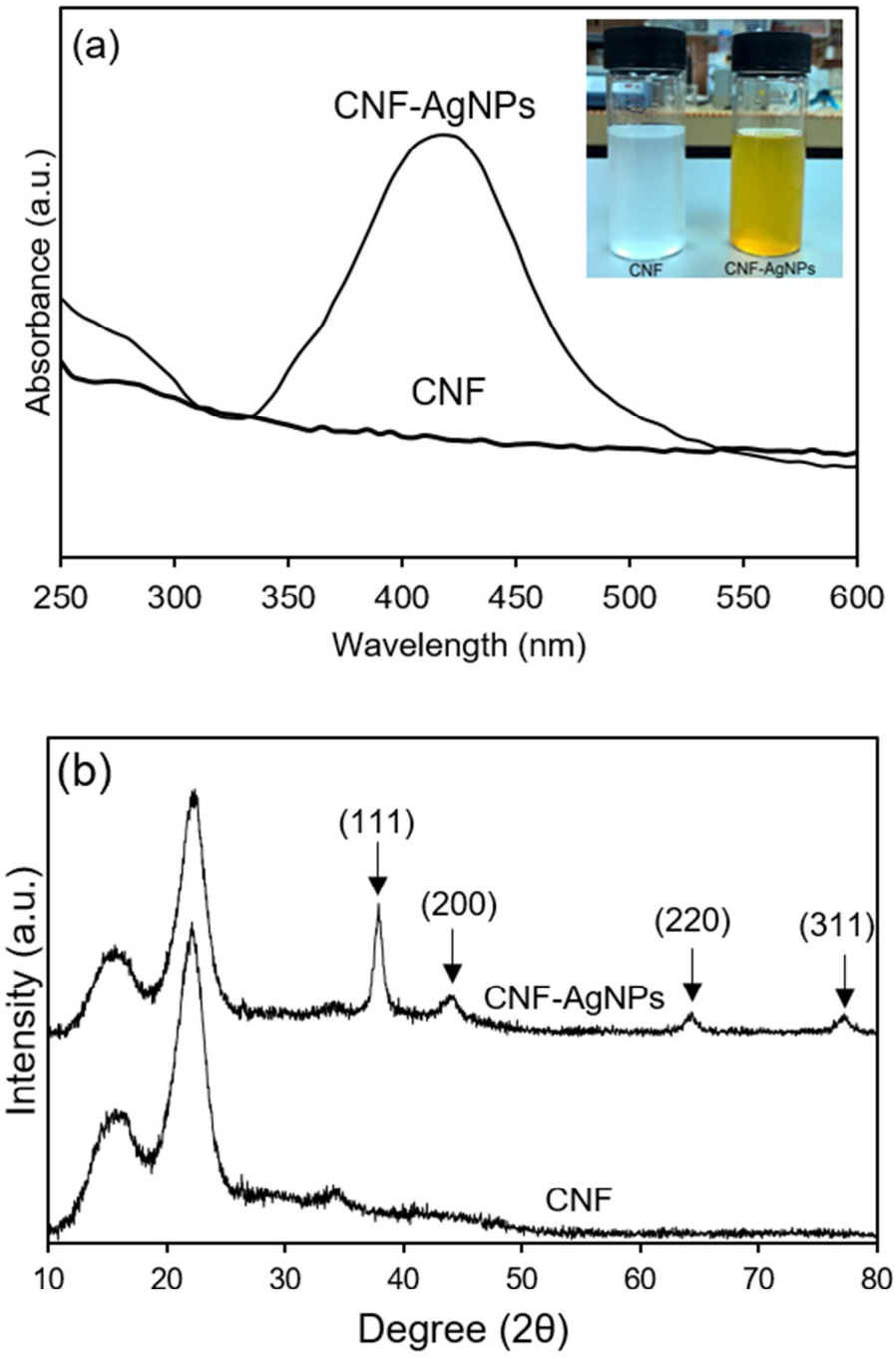

Fig. 1 (a) UV-vis spectra of the CNF and CNF-AgNPs suspensions. The inset shows the transformation of colourless CNF suspension to a yellowish CNF-AgNPs suspension. A clear peak at 420nm is seen, which is indicative of AgNPs formation. (b) XRD diffraction pattern of CNF and CNF-AgNPs.

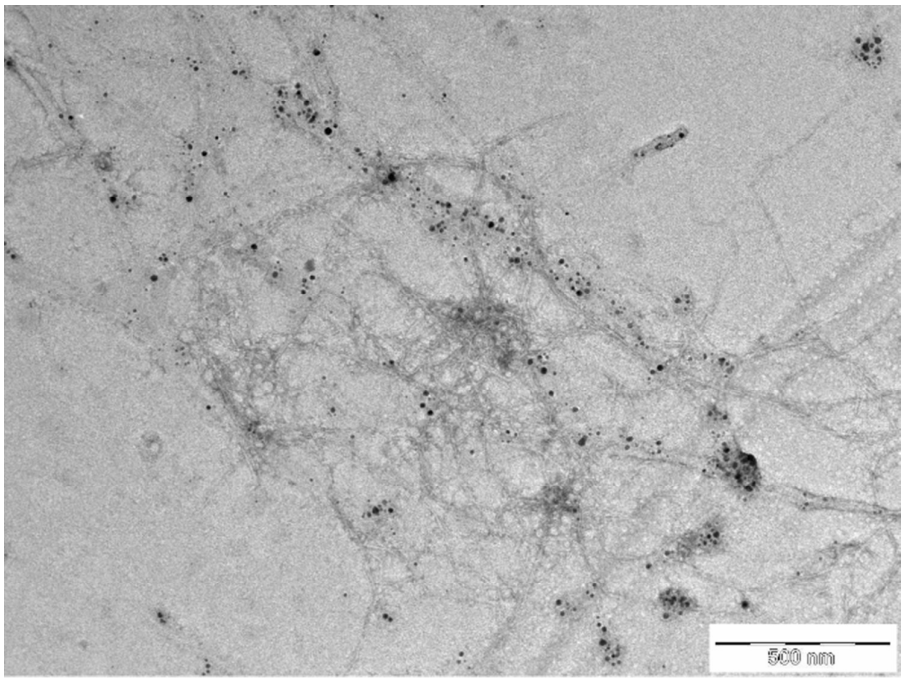

Fig. 2 TEM images of CNF-AgNPs.

The electron micrograph shown in Fig. 2 suggests that the AgNPs, with an average size of 21.62± 3.60 nm, formed via the *in situ* synthesis and attached to the CNF network. It is noted that CNF has played a pivotal role as reducing agent and template for the growth of AgNPs. According to our previous study, CNF contains large numbers of active functional groups, including hydroxyl and carboxyl groups, which originate in the cellulose and hemicelluloses[30]. Furthermore, the high specific surface area of defibrillated CNF maximizes the exposure and interaction of these functional groups with Ag^+ ions during the *in situ* synthesis process. The positively charged Ag^+ ions were electrostatically bound to the negatively charged hydroxyl and carboxyl groups on the CNF, where these active functional groups then served as the nano-nucleation site for AgNPs formation. The reduction of Ag^+ ions was postulated to occur as CNF underwent auto-hydrolysis during the hydrothermal treatment, causing cleavage of cellulose and hemicellulose to generate glucose and xylose. As a result, the reduced zero valence Ag underwent nucleation to form Ag nuclei as Ag^+ ions received electrons from the available reducing sugars.

The CNF-AgNPs suspension was subjected to a low temperature freezing process at –105 ˚C, followed by freeze drying. After the freeze drying process, the CNF-AgNPs had transformed into a sponge-like sample, as illustrated in Fig. 3a. As can been seen in the lower magnification FESEM images in Fig. 3b, the aerogel nanocomposite contained open and porous structures formed by layers of CNF sheets. At a higher magnification (Fig. 3c), tiny pores can be observed on the randomly interconnected CNF network, while clusters of AgNPs (>100 nm) homogeneously decorating the CNF network can also be noted. The frozen and

freeze drying of the CNF-AgNPs suspension resulted in the formation of a highly porous aerogel. The extremely low freezing temperature allowed the water in the CNF-AgNPs suspension to be frozen rapidly and homogeneously. During this stage, a self-assembly process occurred in the CNF involving physical entanglement and intermolecular hydrogen bonding. The subsequent sublimation of water molecules during the freeze drying process left a constructed structure of interconnected CNF, while preventing collapse of the CNF-AgNPs structure upon removal of the ice crystals.

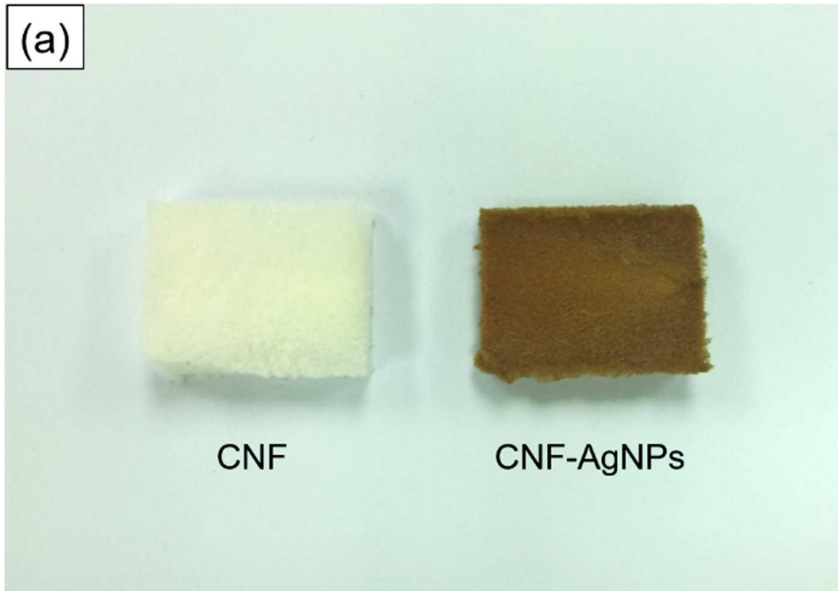

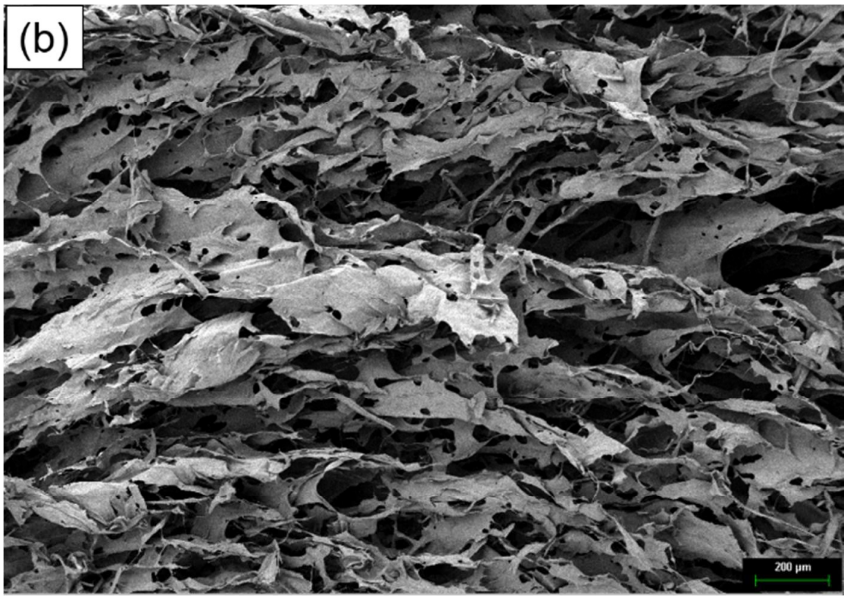

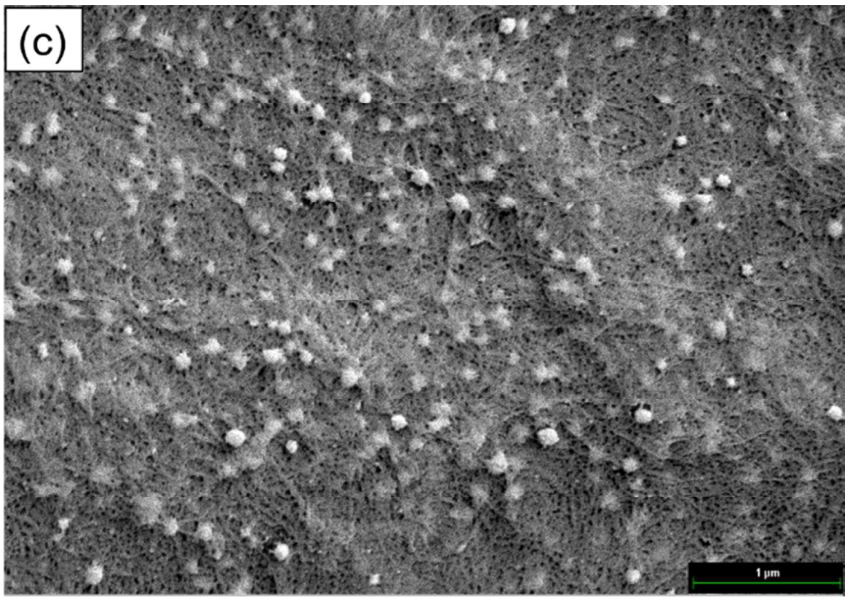

Fig. 3 Digital images of (a) freeze dried CNF and CNF-AgNPs nanocomposite. FESEM images of CNF-AgNPs with (b) lower magnification showing an open structure constructed by the CNF sheets and (c) higher magnification showing surface morphology of the interconnected CNF sheets with tiny pores and immobilized AgNPs clusters.

SERS detection of RhB

Low cost cellulosic-based SERS active substrates, which are flexible, physically and mechanically stable, and ease of use, were fabricated to detect chemical and biological compounds[34-36]. By taking into consideration the capability of CNF for dye up-take, the CNF-AgNPs was used as a SERS substrate for the detection of RhB. The Raman spectra of RhB adsorbed on blank CNF and CNF-AgNPs are illustrated in Fig. 4a. At the same concentration of RhB (5×10^{-3} M), CNF-AgNPs gives an intense signal for the characteristic Raman spectrum of RhB, as compared to the plain CNF. This is mainly attributed to the SERS effect of AgNPs that enhances the scattered signal of RhB. Additionally, the detection sensitivity of the CNF-AgNPs was investigated using different concentrations of RhB ranging from 5×10^{-3} M to 5×10^{-7} M (Fig. 4a). A monotonic increase in the intensity of the Raman spectrum was observed with the increase in concentration of RhB. Several intense peaks at 1647, 1507, 1360, and 1198 cm^{-1} for RhB were still observable at low concentration. A log-log plot of the Raman intensity (based on the peaks mentioned above) versus concentration of RhB yields a linear dependence relationship (Fig. 4b). The highly porous structure of the CNF-AgNPs aerogel nanocomposite is a great advantage for a SERS substrate because it allows the cationic RhB molecule to diffuse and absorb into the porous structure via capillary effect and electrostatic interactions,

respectively. These promoted intimate interactions between AgNPs and RhB molecules. The clusters of AgNPs anchored on the CNF structure could also contribute to the amplification of the scattered Raman signal of RhB through the electromagnetic enhancement mechanism (EM). The EM mechanism is correlated with the LSPR of AgNPs where the incident electromagnetic wave triggered excitation of the free conduction electrons of AgNPs. As a result, this induced enhancement of the electric field of AgNPs that resulted in enhancement of the scattered Raman signal of RhB molecules close to the AgNPs surface[37, 38].

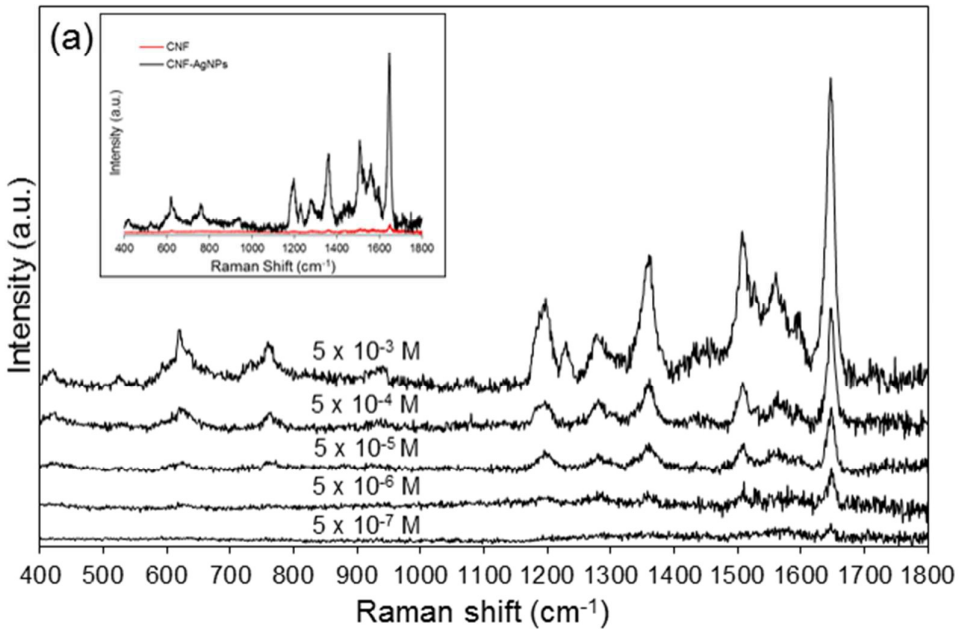

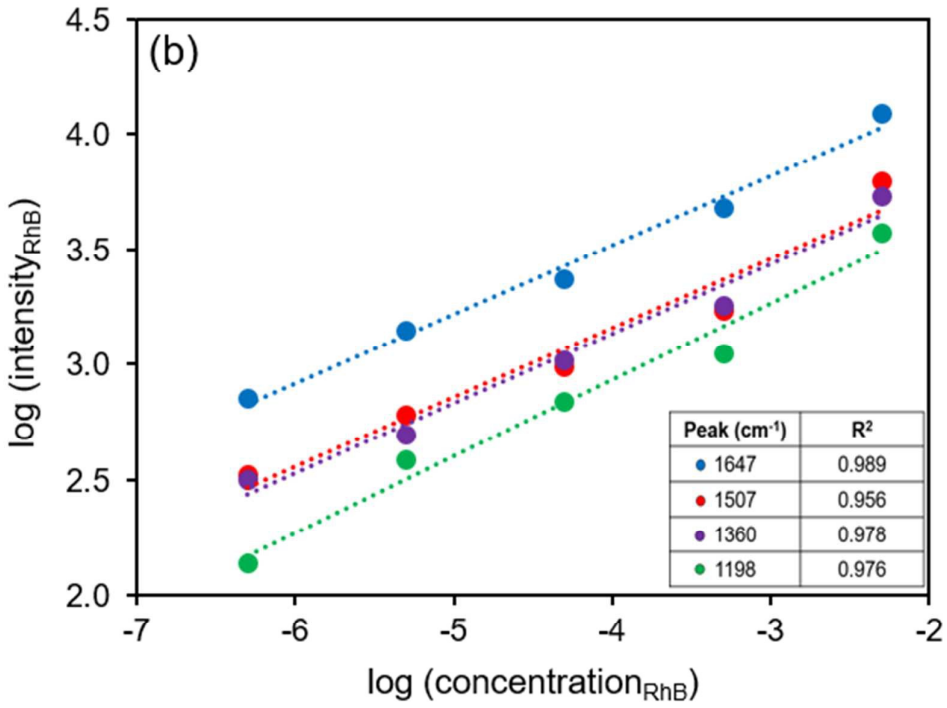

Fig. 4 (a) Raman spectra of RhB at different concentration detected using CNF-AgNPs; the inset is the Raman spectra of 5 × 10^{-3} M RhB adsorbed on CNF (red) and CNF-AgNPs (black). (b) log-log of Raman intensity vs. concentration of RhB at different found peaks.

Catalytic degradation of RhB

Another potential use of CNF-AgNPs nanocomposite was explored via the catalytic degradation of RhB in the presence of $NaBH_4$. The catalytic activity of the nanocomposite was evaluated by varying the weight of CNF-AgNPs (Fig. 5a). The concentration of the RhB was measured based on a calibration curve correlating both concentration and recorded intensity of the UV-vis absorbance at a wavelength of 554 nm. The slight decrease in RhB concentration during the first 5 min of the experiment could be due to the adsorption of RhB onto the CNF. The concentration of RhB decreased rapidly immediately after addition of $NaBH_4$. Complete degradation of RhB can be accomplished within 12 min by use of 10 mg CNF-AgNPs nanocomposite. Further incremental increases in the nanocomposite amount, up to 30 and 60 mg, significantly sped the degradation process, which completed after 8 and 5 min, respectively. Degradation of RhB without CNF-AgNPs nanocomposite was also conducted. As expected, no obvious decolourization of RhB was observed as the absence of the nanocomposites. Moreover, the degradation process was not complete, even after 150 min (see Supplemental Fig. S2). These results indicate that the reducing efficiency of RhB was affected by the amount of AgNPs present as the increase of the nanocomposite favoured the degradation process, while degradation was not completed when the nanocomposite was absent. The degradation of RhB

involved transfer of electrons from sodium borohydride to the dye, however the large difference in redox potential between RhB and BH_4^- restricted the reduction efficiency[39]. In CNF-AgNPs the immobilized AgNPs acted as an intermediate between the large redox potential by relaying the electrons accepted from BH_4^- to catalyse the degradation of the dye molecules[10, 40]. The channels and pores in the CNF-AgNPs aerogel allowed the RhB molecules to diffuse through and increase the interactions between AgNPs, BH_4^-, and RhB. The catalytic degradation performance of $NaBH_4$ with only 10 mg catalyst was also examined using different concentrations of RhB and the results are shown in Fig. 5b. Complete reduction of RhB can be achieved within 5 min and 12 min for 4×10^{-5} M and 1×10^{-4} M RhB, respectively. However, degradation of RhB was limited and not completed after 90 min at a RhB concentration of 2×10^{-4} M.

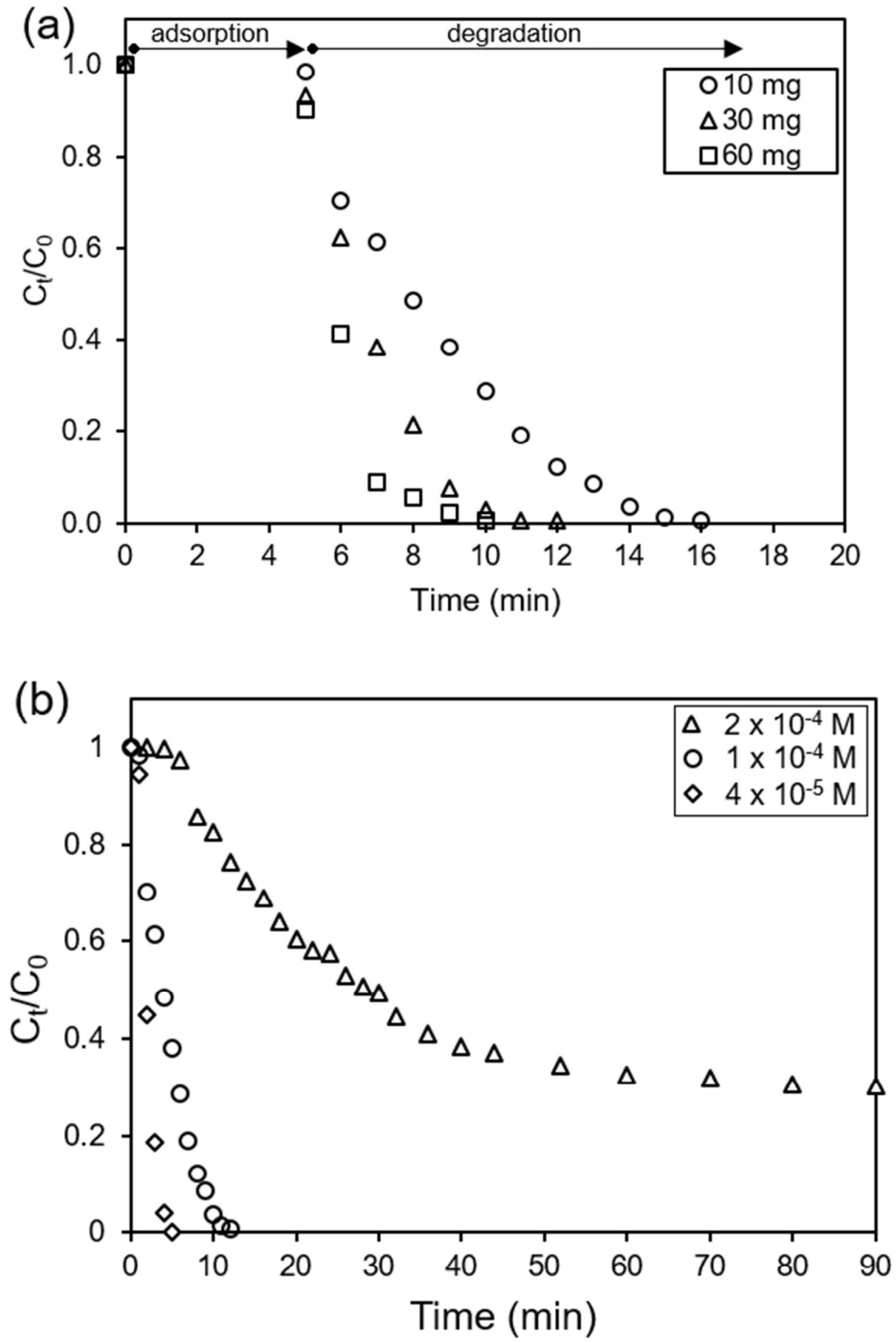

Fig. 5 Plot of C_t/C_0 versus time for (a) dependence of nanocomposite weight on catalytic degradation of RhB and (b) degradation of different concentration of RhB with using 10 mg of CNF-AgNPs aerogel nanocomposite.

Conclusion

In conclusion, a highly porous, functionalized with AgNPs CNF aerogel nanocomposite was fabricated through an environmentally benign method. The

inexpensive, hydrophilic, and high specific surface nanocellulose was used as a substrate material for reduction and immobilizations of AgNPs owing to its abundant and highly reactive functional groups. The CNF-AgNPs nanocomposite demonstrated SERS activity and catalytic properties, which can be used for effective detection and degradation of dyes with potential applications in environment remediation.

Acknowledgement
The authors acknowledge the financial support provided by the research project grants of DIP-2014-013 and LRGS/TD/2012/USM-UKM/PT/04.

References

1. G. Crini, *Bioresour. Technol.*, 2006, **97**, 1061-1085.
2. M. Rafatullah, O. Sulaiman, R. Hashim and A. Ahmad, *J. Hazard. Mater.*, 2010, **177**, 70-80.
3. J. Li, T. Zhao, T. Chen, Y. Liu, C. N. Ong and J. Xie, *Nanoscale*, 2015, **7**, 7502-7519.
4. M. M. Khin, A. S. Nair, V. J. Babu, R. Murugan and S. Ramakrishna, *Energy Environ. Sci.*, 2012, **5**, 8075-8109.
5. N. Savage and M. Diallo, *J. Nanopart. Res.*, 2005, **7**, 331-342.
6. Q. Li, S. Mahendra, D. Y. Lyon, L. Brunet, M. V. Liga, D. Li and P. J. J. Alvarez, *Water Res.*, 2008, **42**, 4591-4602.
7. T. A. Dankovich and D. G. Gray, *Environ. Sci. Technol.*, 2011, **45**, 1992-1998.
8. M. Rycenga, P. H. C. Camargo, W. Li, C. H. Moran and Y. Xia, *J. Phys. Chem. Lett.*, 2010, **1**, 696-703.
9. B. Sharma, R. R. Frontiera, A.-I. Henry, E. Ringe and R. P. Van Duyne, *Mater. Today*, 2012, **15**, 16-25.
10. Z.-J. Jiang, C.-Y. Liu and L.-W. Sun, *J. Phys. Chem. B*, 2005, **109**, 1730-1735.
11. Y. Zheng and A. Wang, *J. Mater. Chem.*, 2012, **22**, 16552-16559.
12. L. Ai and J. Jiang, *Bioresour. Technol.*, 2013, **132**, 374-377.
13. B. Baruah, G. J. Gabriel, M. J. Akbashev and M. E. Booher, *Langmuir*, 2013, **29**, 4225-4234.
14. S. W. Chook, C. H. Chia, S. Zakaria, M. K. Ayob, N. M. Huang, H. M. Neoh and R. Jamal, *RSC Adv.*, 2015, **5**, 26263-26268.
15. M. R. de Moura, L. H. C. Mattoso and V. Zucolotto, *J. Food Eng.*, 2012, **109**, 520-524.
16. J. He, T. Kunitake and A. Nakao, *Chem. Mat.*, 2003, **15**, 4401-4406.
17. M. Montazer, F. Alimohammadi, A. Shamei and M. K. Rahimi, *Carbohydr. Polym.*, 2012, **87**, 1706-1712.
18. Z. Li, L. Wang, S. Chen, C. Feng, S. Chen, N. Yin, J. Yang, H. Wang and Y. Xu, *Cellulose*, 2015, **22**, 373-383.
19. J. Cai, S. Kimura, M. Wada and S. Kuga, *Biomacromolecules*, 2008, **10**, 87-94.
20. V. Chumachenko, N. Kutsevol, M. Rawiso, M. Schmutz and C. Blanck, *Nanoscale Res. Lett.*, 2014, **9**, 164.
21. M. A. El-Sheikh, S. M. El-Rafie, E. S. Abdel-Halim and M. H. El-Rafie, *j. Polym.*, 2013, **2013**, 11.

22. R. Xiong, C. Lu, W. Zhang, Z. Zhou and X. Zhang, *Carbohydr. Polym.*, 2013, **95**, 214-219.
23. N. Drogat, R. Granet, V. Sol, A. Memmi, N. Saad, C. Klein Koerkamp, P. Bressollier and P. Krausz, *J. Nanopart. Res.*, 2011, **13**, 1557-1562.
24. M. S. Wang, F. Jiang, Y.-L. Hsieh and N. Nitin, *J. Mater. Chem. B*, 2014, **2**, 6226-6235.
25. H. Dong, J. F. Snyder, D. T. Tran and J. L. Leadore, *Carbohydr. Polym.*, 2013, **95**, 760-767.
26. T. Saito, Y. Nishiyama, J.-L. Putaux, M. Vignon and A. Isogai, *Biomacromolecules*, 2006, **7**, 1687-1691.
27. H. Liimatainen, M. Visanko, J. A. Sirviö, O. E. O. Hormi and J. Niinimaki, *Biomacromolecules*, 2012, **13**, 1592-1597.
28. K. Parikka, A.-S. Leppänen, C. Xu, L. Pitkänen, P. Eronen, M. Österberg, H. Brumer, S. Willför and M. Tenkanen, *Biomacromolecules*, 2012, **13**, 2418-2428.
29. S. Iwamoto, K. Abe and H. Yano, *Biomacromolecules*, 2008, **9**, 1022-1026.
30. C. H. Chan, C. H. Chia, S. Zakaria, M. S. Sajab and S. X. Chin, *RSC Adv.*, 2015, **5**, 18204-18212.
31. M. Mohammadi, A. J. Hassani, A. R. Mohamed and G. D. Najafpour, *J. Chem. Eng. Data*, 2010, **55**, 5777-5785.
32. K. Shakir, A. F. Elkafrawy, H. F. Ghoneimy, S. G. Elrab Beheir and M. Refaat, *Water Res.*, 2010, **44**, 1449-1461.
33. E. Hutter and J. H. Fendler, *Adv. Mater.*, 2004, **16**, 1685-1706.
34. M.-L. Cheng, B.-C. Tsai and J. Yang, *Anal. Chim. Acta*, 2011, **708**, 89-96.
35. C. H. Lee, M. E. Hankus, L. Tian, P. M. Pellegrino and S. Singamaneni, *Anal. Chem.*, 2011, **83**, 8953-8958.
36. L. Polavarapu and L. M. Liz-Marzan, *Phys. Chem. Chem. Phys.*, 2013, **15**, 5288-5300.
37. S. Schlücker, *Angew. Chem., Int. Ed.*, 2014, **53**, 4756-4795.
38. Z. Xu and G. Hu, *RSC Adv.*, 2012, **2**, 11404-11409.
39. K. Mallick, M. Witcomb and M. Scurrell, *Mater. Chem. Phys.*, 2006, **97**, 283-287.
40. V. K. Vidhu and D. Philip, *Micron*, 2014, **56**, 54-62.